Topological Characterization of Fractional Quantum Hall Ground States from Microscopic Hamiltonians

Michael P. Zaletel, Roger S. K. Mong, and Frank Pollmann

Topological characterization of fractional quantum Hall ground states from microscopic Hamiltonians

Michael P. Zaletel,[1] Roger S. K. Mong,[1, 2] and Frank Pollmann[3]

[1]*Department of Physics, University of California, Berkeley, California 94720, USA*
[2]*Department of Physics, California Institute of Technology, Pasadena, California 91125, USA*
[3]*Max-Planck-Institut für Physik komplexer Systeme, 01187 Dresden, Germany*

We show how to numerically calculate several quantities that characterize topological order starting from a microscopic fractional quantum Hall (FQH) Hamiltonian. To find the set of degenerate ground states (GS), we employ the infinite density matrix renormalization group (iDMRG) method based on the matrix-product state (MPS) representation of FQH states on an infinite cylinder. To study localized quasiparticles of a chosen topological charge, we use pairs of degenerate GSs as boundary conditions for the iDMRG. We then show that the wave function obtained on the infinite cylinder geometry can be adapted to a torus of arbitrary modular parameter, which allows us to explicitly calculate the non-Abelian Berry connection associated with the modular $\mathcal{T}$-transformation. As a result, the quantum dimensions, topological spins, quasiparticle charges, chiral central charge, and Hall viscosity of the phase can be obtained using data contained entirely in the entanglement spectrum of an infinite cylinder.

Over the last decades several new kinds of phases have been discovered which cannot be characterized by spontaneous symmetry breaking, but instead exhibit *topological order* [1, 2]. A prominent example of a topological ordered phase is the fractional quantum Hall (FQH) effect [3]. These systems support quasiparticles (QPs) with exotic exchange statistics (*i.e.*, they are neither fermions nor bosons), and have been proposed as a platform for a 'topological' quantum computer [4–7]. Exact diagonalization (ED) numerics have played a decisive role in the study of FQH phases [8–10], and many characteristics of the topological order can be extracted directly from the ground states (GSs) via their entanglement structure [11–16]. However, the exponential growth of the Hilbert space as a function of particle number means that ED is prohibitively expensive beyond ≈ 20 particles. While it is possible to obtain very accurate results for some systems with a small correlation length, such as the $\nu = 1/3$ Coulomb state, more complicated systems (system with higher Landau level, hierarchy states, or non-Abelian phases) are much harder to access and finite size effects are much stronger.

In this paper we address the limitations of ED by using the infinite density matrix renormalization group (iDMRG) algorithm to obtain the matrix product state (MPS) representation of the GSs of FQH Hamiltonians on *infinitely* long cylinders with finite circumference L (see Fig. 1). The space of MPSs has been shown to be an exact and efficient representation of the model QH states [17, 18]; iDMRG extends these results to non-model states by variationally optimizing an MPS with respect to a microscopic Hamiltonian [19]. For a system of size $L_x \times L_y$, *finite* DMRG reduces the computational complexity from $\mathcal{O}(b^{L_x L_y})$ via ED to $\mathcal{O}(L_x L_y b^{L_x})$, with $b \gtrsim 1$; taking $L_y \to \infty$ using *infinite* DMRG gives $\mathcal{O}(b^{L_x})$. Several groups have by now implemented finite DMRG to simulate FQH Hamiltonians [20–25]. The in-
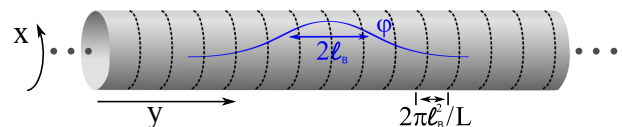

FIG. 1. Single particle states $\varphi(x, y)$ in the lowest Landau level of an infinite cylinder. L is the circumference of the cylinder and ℓ_B is the magnetic length.

finite cylinder geometry has several additional numerical advantages, such as translation invariance both along and around the cylinder, zero curvature effects [25], and the absence of gapless edge excitations which slow down the convergence. In contrast to the standard bipartition of the torus [14, 26, 27], cutting the infinite cylinder gives the entanglement spectrum of a single edge.

We demonstrate how to obtain various characterizing quantities of quantum Hall systems from microscopic Hamiltonians using the iDMRG simulations. Like the torus, the infinite cylinder has topologically degenerate ground states, which we systemically obtain in the MPS representation using iDMRG. In addition to the QP quantum dimensions d_a [11, 12, 28], we also show how to extract their charges and topological spins, the chiral central charge of the edge conformal field theory (CFT), and the Hall viscosity of the bulk using only the entanglement spectra. By forming domain walls between pairs of degenerate GSs, we obtain the energy and MPS of a localized QP of a chosen topological charge. We apply the infinite cylinder technique to spin-polarized electrons at filling $\nu = 1/3$, 2/5 and 1/2.

Recently Cincio and Vidal [29] applied iDMRG to a lattice Hamiltonian on a cylinder and extracted the braiding statistics of the anyons ('$\mathcal{S}$' and '$\mathcal{T}$') using wavefunction overlaps [16]. In this work we employ iDMRG to continuum FQH Hamiltonians and extract topological information purely from the entanglement spectra.

Model and method. We consider the cylinder geometry [30–32] with a coordinate x running around the circumference of length L, and y running along the infinite length of the cylinder (see Fig. 1). The Landau gauge $\mathbf{A} = \ell_B^{-2}(-y, 0)$ conserves the x-momentum around the cylinder. The orbitals in the first Landau level are

$$\varphi_n(x, y) = \frac{e^{ik_n x - \frac{1}{2\ell_B^2}(y - k_n \ell_B^2)^2}}{\sqrt{L \ell_B \pi^{1/2}}}, \quad k_n = \frac{2\pi n}{L}, \quad (1)$$

where $n \in \mathbb{Z}$, with a density of one orbital per flux-quanta. Because each orbital is localized at $y_n = k_n \ell_B^2$, we treat the system as a 1D chain. The most general two-body interaction allowed by translational symmetry can be specified by coefficients V_{km},

$$\hat{H} = \sum_n \sum_{k \geq |m|} V_{km} c_{n+m}^\dagger c_{n+k}^\dagger c_{n+m+k} c_n. \quad (2)$$

If the interactions are local in real space, they will be Gaussian localized with a range on the order of L/ℓ_B in the chain representation. The Hamiltonian can be parameterized by the set of 'Haldane pseudopotentials' V_m which can represent any rotationally and translationally invariant two-body interaction within a single Landau level. For example, the hard core Haldane pseudopotential V_1 takes the form $V_{km} \propto (k^2 - m^2)e^{-\frac{1}{2}(2\pi \ell_B/L)^2(k^2+m^2)}$ [30]. To represent $\hat{H}$ at some fixed accuracy we must keep $\mathcal{O}(L^2/\ell_B^2)$ terms in the Hamiltonian.

For our numerical simulations, we use the iDMRG algorithm [33] which is based on the MPS representation,

$$|\Psi\rangle = \sum_{\{j_n\}} \left[\cdots B^{[0]j_0} B^{[1]j_1} \cdots \right] |\ldots, j_0, j_1, \ldots\rangle, \quad (3)$$

where $B^{[n]j_n}$ are $\chi \times \chi$ matrices and $|j_n\rangle$, $j_n \in \{0, 1\}$ represent the occupancy at orbital n. Assuming the state $|\Psi\rangle$ is translationally invariant with a unit cell of length M, then we need only store M different tensors $B^{[i]}$ to express the MPS, *i.e.*, $B^{[i]} = B^{[i+M]}$; at filling $\nu = p/q$, M must be a multiple of q. MPS have proven to be extremely successful in the simulation of gapped, one-dimensional systems because their GSs can be expressed to very high accuracy by keeping a relatively small χ even for infinite system size [34–37]. The iDMRG algorithm proceeds by iteratively minimizing $E = \langle \Psi | \hat{H} | \Psi \rangle$ within the space of MPS. The χ needed to express the ground state to a given accuracy grows exponentially with L; a moderate bond dimension of $\chi = 3600$ was sufficient for the largest system considered here, which took under a day. In the Supplementary material we address several technical issues particular to QH iDMRG [38].

We incorporate both particle number and momentum conservation in the MPS representation and iDMRG algorithm [39], which assume an important role in the subsequent analysis. The quantum numbers are defined to
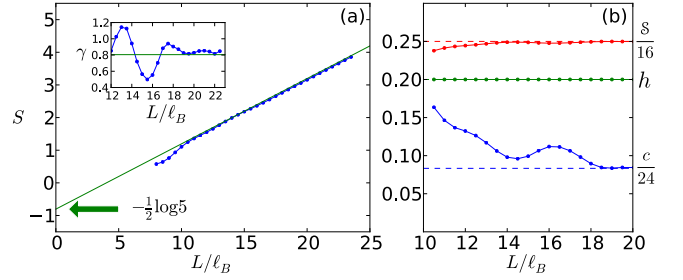

FIG. 2. (Color online) (a) Entanglement entropy S of the $\nu = 2/5$ state as a function of the circumference L, for a bipartition into two half-infinite cylinders. The inset shows the estimated TEE $\gamma = L\frac{dS}{dL} - S(L)$ converging to $\gamma = \frac{1}{2} \log 5$ (green line) for large L. (b) Estimate of the chiral central charge $c/24$, the topological spin h of the $e/5$ QP, and the Hall viscosity as expressed through the 'shift', $\mathcal{S} = \frac{8\pi \ell_B^2}{\hbar \nu} \eta_H$ [40]. Dashed lines show expected hierarchy values of $2/24$, $1/5$, $4/16$ respectively. That h is identically correct is peculiar to abelian QPs.

be

$$\hat{C} = \sum_n \hat{C}_n \equiv \sum_n (\hat{N}_n - \nu) \quad \text{(particle number)}, \quad (4a)$$

$$\hat{K} = \sum_n \hat{K}_n \equiv \sum_n n(\hat{N}_n - \nu) \quad \text{(momentum)}, \quad (4b)$$

where $\hat{N}_n$ is the number operator at site n.

The Schmidt states $|\alpha\rangle_{L/R}$ of $|\Psi\rangle$ on bond $\bar{n}$ form orthonormal bases for the sites to the left and right of the bond, with corresponding Schmidt values $\lambda_{\bar{n};\alpha}$. They have a well defined particle number $\bar{C}_{\bar{n};\alpha}$ representing the total charge to the left of bond $\bar{n}$. We will view $\bar{C}_{\bar{n}}$ as a diagonal matrix acting in the set of Schmidt states (as for $\bar{K}$). It will prove useful to define a 'bond expectation value,' $\langle \bar{C}_{\bar{n}} \rangle \equiv \sum_\alpha \lambda_{\bar{n};\alpha}^2 \bar{C}_{\bar{n};\alpha}$, which gives the expected value of the charge to the left of bond $\bar{n}$ (as for $\bar{K}$). The Schmidt values and their quantum numbers, $(\lambda, \bar{C}, \bar{K})_{\bar{n}}$, constitute the 'orbital entanglement spectrum' (OES) of the bond. The corresponding entanglement entropy is defined as $S_{\bar{n}} \equiv -\sum_\alpha \lambda_{\bar{n};\alpha}^2 \log \lambda_{\bar{n};\alpha}^2$.

Topological order and QPs. We now recall some basic facts about topological order on a cylinder [41]. A topologically ordered state with $\mathfrak{m}$ QP types (labeled by 'a') has an $\mathfrak{m}$-fold GS degeneracy on an infinite cylinder. The chiral CFT describing the edge contains $\mathfrak{m}$ scaling operators $\{\phi_a\}$ which insert a corresponding QP a near the edge. The Hilbert space of the edge $\mathcal{H}$ can be decomposed into a direct sum of subspaces $\mathcal{H}_a$ that contain the edge states with topological charge a. In addition, the states of the low-lying OES are in one-to-one correspondence with the states of the edge CFT [11, 13]. With an entanglement cut running around the circumference of the cylinder, we can choose a particular basis $\{|\Xi_a\rangle\}$ for the $\mathfrak{m}$-dimensional vector space of GSs such that the low-lying part of the OES of $|\Xi_a\rangle$ contains states *only* in $\mathcal{H}_a$. As each $|\Xi_a\rangle$ contains fewer states in the low-energy

part of the OES than the full CFT, they have lower entanglement entropy and are referred to as the 'minimal entanglement states' (MESs) [16]. Translations permute the MESs, so the OES of a state depends on the bond $\bar{n}$ between adjacent orbitals where the cylinder is cut. Consequently each bond $\bar{n}$ is labeled by the sector a found in its OES; we therefore denote the corresponding bond by $\bar{a}$ [42].

We now outline the procedure for finding the full set of degenerate GSs using iDMRG. On an infinite cylinder the MESs are energy eigenstates, possibly with a degeneracy split exponentially in L [29]. Furthermore, for QH problems in a topological phase, initializing the iDMRG using an orbital configuration 'μ' (for example, $\mu = 010$ gives $|\cdots 010010 \cdots \rangle$) should generate the set of distinct MES after iDMRG optimization. For many QH states, this is a consequence of MESs' distinct quantum numbers K, though we suspect the result is more general [38]. If we find optimized energies such that $E_{\mu_1} < E_{\mu_2}$, then the state derived from initial state μ_2 is rejected. The iDMRG is the numerical check that a given μ leads to one of the $\mathfrak{m}$ GSs.

The entanglement entropy of each MES $|\Xi_a\rangle$ scales with the circumference as $S \approx sL - \gamma_a$, where $\gamma_a = \log \sqrt{\sum_b d_b^2} - \log(d_a)$ are the topological entanglement entropies (TEEs) and d_a are the quantum dimensions of the QPs [11, 12, 28]. From the TEEs γ_a we can determine if we have the complete set of MESs [29]. As an example of an Abelian model ($d_a = 1$ for all a), we consider $\nu = 2/5$ filling for Haldane pseudopotentials $V_3/V_1 = 0.05$, for which the seed $|01010\rangle$ and its translates were numerically determined to provide the 5 MESs. This has been considered before in an ED study with Coulomb interactions on a torus for circumferences up to $L = 18\ell_B$ [14], from which it was difficult to determine γ accurately. We are able to go up to $L = 23.5\ell_B$ and obtain the results shown in Fig. 2. The estimated TEE is $\gamma \approx 0.83$ (close to $\frac{1}{2}\log 5 \approx 0.8047$).

As an example which has a non-Abelian phase, we consider the filling $\nu = 1/2$ which contains both the gapless composite Fermi liquid (CFL) phase and the gapped, non-Abelian MR phase [41, 43]. Using a sum of Haldane pseudopotentials V_1 and V_3, we tune between the CFL (small V_3/V_1) and MR (intermediate V_3/V_1) phases. We start the iDMRG either with the $|0110\rangle$ configuration (which provides four states via translation) or $|0101\rangle$ (which provides two). We observe that in the suspected CFL phase the energies of the two sectors are split, while the MR phase is nearly 6-fold degenerate, as illustrated in Fig. 3(a). Fixing a point in the MR phase, the difference in the entanglement entropies of the MESs is $S_{0101} - S_{0110} \approx 0.36$, which implies that the S_{0101} state is associated with a non-Abelian particle of quantum dimension 1.43 (close to that of the $e/4$ excitation: $\sqrt{2} \approx 1.41$), as illustrated in Fig. 3(b). This supports the non-Abelian nature of the state.
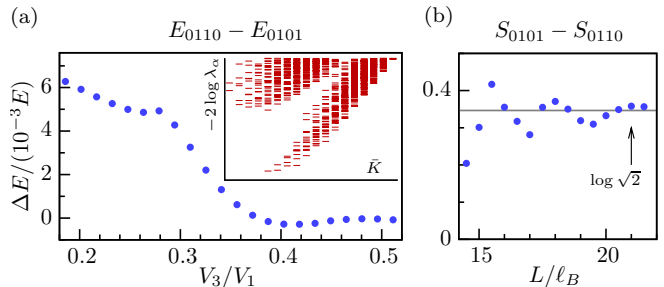

FIG. 3. (a) The relative energy difference between states in the 0110 and 0101 sectors at $\nu = 1/2$ filling and $L = 16\ell_B$, plot against the ratio of pseudopotential strengths V_3/V_1. At small V_3/V_1, the energies $E_{0110} > E_{0101}$ and hence there is only a two-fold GS degeneracy (CFL phase), whereas at large V_3/V_1 the energies are roughly equal which give rise to a six fold GS degeneracy (MR phase). Inset shows the real-space entanglement spectrum of the 0101 state plotted versus $\bar{K}$.(b) Fixing a point $V_3/V_1 = 0.4$ in the MR phase, we increase L and measure the difference in entanglement entropies $S_{0101} - S_{0110}$. The result is consistent with $d_\sigma = \sqrt{2}$ for the $e/4$ QP.
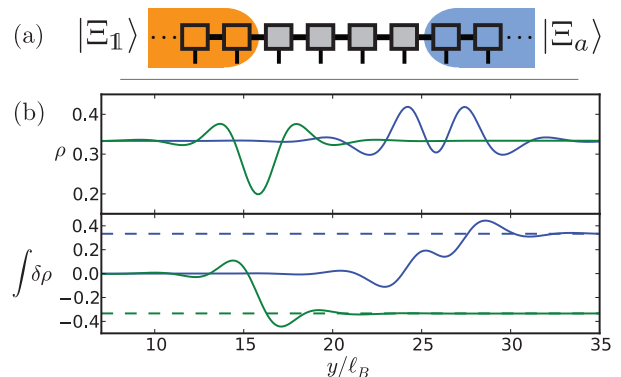

FIG. 4. (color online) (a) The MPS used to represent a QP 'a'. (b) The charge density $\rho(y)$ of the numerically optimized QP with charge $+e/3$ (blue line) and $-e/3$ (green line) of the $\nu = 1/3$ state. The cylinder has circumference $L = 16\ell_B$ and the potential approximates a dipolar r^{-3} interaction.

In the cylinder geometry, the QPs appear as domain walls between the degenerate GSs. To generate a QP of type a in the vicinity of $y = 0$, we use the B-matrices of the identity MPS $|\Xi_\mathbb{1}\rangle$ for sites at $y \ll 0$ and the B-matrices of $|\Xi_a\rangle$ for $y \gg 0$. In the vicinity of $y = 0$, we insert a finite number of B-matrices which we numerically optimize. For efficiency we work with QPs of fixed momentum K; the resulting QPs for the $\nu = 1/3$ state are illustrated in Fig. 4. To calculate the charge of the particle we measure $Q_a = \lim_{\epsilon \to 0} \sum_n e^{-\epsilon |n|} \hat{C}_n$, where $\hat{C}_n$ is the on-site charge operator defined in Eq. (4). The resulting charge is in fact *independent* of the B-matrices used to glue together the MPS; Q_a can be calculated exactly knowing only the OES of the infinite MPS $|\Xi_a\rangle$ using $e^{2\pi i Q_a} = e^{2\pi i(\langle\langle \bar{C}\rangle\rangle - \bar{C}_{\bar{a}})}$, where $\langle\langle \bar{C}\rangle\rangle$ is the average of $\langle \bar{C}_{\bar{n}}\rangle$ over *all* bonds $\bar{n}$ in the MPS of $|\Xi_a\rangle$ [42]. This
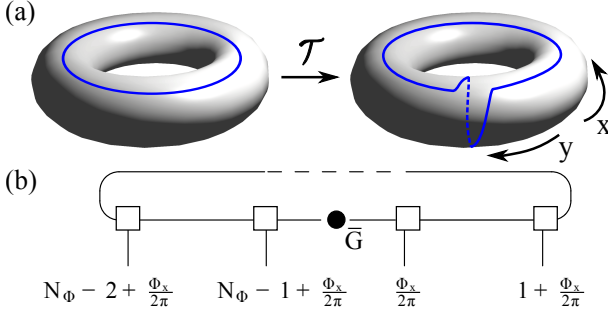
FIG. 5. (a) A torus with dimensions $L_x \times L_y$. Taking the modular parameter $\tau \to \tau + 1$ generates a modular transform '$\mathcal{T}$' of the torus, and acts on the set of GSs as a matrix U_T. (b) The wavefunction on the torus is represented by a periodic MPS. The sites are labelled by $n \in \mathbb{Z} + \frac{\Phi_x}{2\pi}$ due the flux threading in the x-direction.

expression is exact and reduces to the 'pattern of zeros' result in the limit of a thin cylinder [44].

Ground states on a torus and topological spin. Several quantities of interest, such as the phase's response to flux insertion and modular transformations, are defined on the torus geometry, so it is useful to convert the cylinder MPS to a torus MPS. The torus is made by taking a cylinder of circumference L_x and identifying points (x, y) to $(x + \tau_x L_x, y + L_y)$, where $\tau = \tau_x + iL_y/L_x$ is the modular parameter. We also allow fluxes $\Phi_{x/y}$ to thread through the two cycles. For a suitable definition of the $N_\Phi = L_x L_y / 2\pi \ell_B^2$ orbitals of the torus [38], we can construct wavefunctions on the torus from those on the infinite cylinder by taking a finite segment of the cylinder MPS and connecting the two edge auxiliary bonds together to form a ring [29], as illustrated in Fig. 5(b). There is no need to reoptimize the B-matrices near the seam: locally the torus Hamiltonian is identical to that of an infinite cylinder, and if L_y is greater than the correlation length the periodic MPS will have the same local correlations as the iMPS. The fluxes and modular parameter can be accounted for by inserting a diagonal matrix $\bar{G}$ when connecting the two edge auxiliary bonds [38],

$$\bar{G} = (-1)^{(N^e - 1)\bar{C}} \, e^{-2\pi i \tau_x \bar{K}} \, e^{i \Phi_y \bar{C}}, \qquad (5)$$

where $\bar{C}$ and $\bar{K}$ are the conserved particle number and momentum of the Schmidt states and N^e is the total particle number. The first factor enforces fermion statistics of the orbitals, the second factor adds a $2\pi\tau_x$ twist when connecting the ends of a cylinder, and the final factor arises from the flux Φ_y threaded through the y-direction. Via this construction we obtain the set of MESs on a torus $|\Xi_a\rangle$ for arbitrary τ and $\Phi_{x/y}$. By adiabatically varying these parameters, we obtain the associated Berry phases characteristic of the topological order.

The Berry phase U_T calculated as τ_x goes from 0 to 1 [45] corresponds to a '$\mathcal{T}$-transformation' of the torus as shown in Fig. 5(a). U_T is diagonal in the MES basis,

and we expect it to contain two contributions [Eq. (6a)]. First, when acting on $|\Xi_a\rangle$, $\mathcal{T}$ causes an anyonic flux a to wind once around the x-cycle of the torus, generating a phase $h_a - \frac{c}{24}$, where h_a is the spin of a and c is the chiral central charge of the edge theory. Second, shearing the bulk introduces a phase due to the universal 'Hall viscosity' η_H of the fluid [40, 46]. U_T can be calculated exactly by making use of the torus MPS [Eq. (5)], and we find that the result depends only on the infinite cylinder OES [Eq. (6b)]. Equating the expected and exact results, for fermions we find

$$U_{T;ab} = \delta_{ab} \exp\left[2\pi i \left(h_a - \frac{c}{24} - \frac{\eta_H}{2\pi\hbar} L_x^2\right)\right] \qquad (6a)$$

$$= \delta_{ab} \, e^{2\pi i \left(\bar{K}_{\bar{a}} - \langle\langle \bar{K} - \bar{n}\bar{C}\rangle\rangle - \nu/24 - \frac{\nu L_x^2}{16\pi^2 \ell_B^2}\right)}. \qquad (6b)$$

In Fig. 2(b), we use the $\nu = 2/5$ OES obtained from iDMRG to extract h, c and η_H, and find good agreement with the expected values for the Abelian hierarchy state [47]. For the MR phase, we obtain excellent results for the model Hamiltonian [38], but when using only the two-body V_m, the measurement is highly sensitive to tunneling between the Pfaffian and anti-Pfaffian states present at the sizes studied [48, 49].

Conclusions. In this paper we showed how to numerically calculate several quantities which characterize topological order starting from a microscopic FQH Hamiltonian. The approach consists of two key steps: (i) We find the MPSs representation of a complete set of GSs using an iDMRG algorithm. (ii) We derived expressions for the QP charges, topological spins, chiral central charge, and Hall viscosity of the phase from the MPS representation.

Independently, Cincio and Vidal have developed a similar technique for using DMRG to probe quasiparticles [50]. Also Tu, Zhang and Qi reported a similar method for extracting the topological spin from entanglement [51].

---

[1] X.-G. Wen, Int. J. Mod. Phys. **B4**, 239 (1990).
[2] X. G. Wen and Q. Niu, Phys. Rev. B **41**, 9377 (1990).
[3] D. C. Tsui, H. L. Stormer, and A. C. Gossard, Phys. Rev. Lett. **48**, 1559 (1982).
[4] A. Y. Kitaev, Ann. Phys. **303**, 2 (2003).
[5] S. Das Sarma, M. Freedman, and C. Nayak, Phys. Rev. Lett. **94**, 166802 (2005).

[6] P. Bonderson, A. Kitaev, and K. Shtengel, Phys. Rev. Lett. **96**, 016803 (2006).

[7] C. Nayak, S. H. Simon, A. Stern, M. Freedman, and S. Das Sarma, Rev. Mod. Phys. **80**, 1083 (2008).

[8] R. B. Laughlin, Phys. Rev. Lett. **50**, 1395 (1983).

[9] D. Yoshioka, B. I. Halperin, and P. A. Lee, Phys. Rev. Lett. **50**, 1219 (1983).

[10] F. D. M. Haldane, Phys. Rev. Lett. **51**, 605 (1983).

[11] A. Kitaev and J. Preskill, Phys. Rev. Lett. **96**, 110404 (2006).

[12] M. Levin and X.-G. Wen, Phys. Rev. Lett. **96**, 110405 (2006).

[13] H. Li and F. D. M. Haldane, Phys. Rev. Lett. **101**, 010504 (2008).

[14] A. M. Laeuchli, E. J. Bergholtz, and M. Haque, New J. Phys. **12**, 075004 (2010).

[15] Z. Papić, B. A. Bernevig, and N. Regnault, Phys. Rev. Lett. **106**, 056801 (2011).

[16] Y. Zhang, T. Grover, A. Turner, M. Oshikawa, and A. Vishwanath, Phys. Rev. B **85**, 235151 (2012).

[17] M. P. Zaletel and R. S. K. Mong, Phys. Rev. B **86**, 245305 (2012).

[18] B. Estienne, Z. Papic, N. Regnault, and B. A. Bernevig, ArXiv e-prints (2012), arXiv:1211.3353 [cond-mat.str-el].

[19] S. R. White, Phys. Rev. Lett. **69**, 2863 (1992).

[20] N. Shibata and D. Yoshioka, Phys. Rev. Lett. **86**, 5755 (2001).

[21] E. J. Bergholtz and A. Karlhede, "Density Matrix Renormalization Group Study of a Lowest Landau Level Electron Gas on a Thin Cylinder," (2003), unpublished, arXiv:cond-mat/0304517.

[22] A. E. Feiguin, E. Rezayi, C. Nayak, and S. Das Sarma, Phys. Rev. Lett. **100**, 166803 (2008).

[23] D. L. Kovrizhin, Phys. Rev. B **81**, 125130 (2010).

[24] J. Zhao, D. N. Sheng, and F. D. M. Haldane, Phys. Rev. B **83**, 195135 (2011).

[25] Z.-X. Hu, Z. Papic, S. Johri, R. Bhatt, and P. Schmitteckert, Physics Letters A **376**, 2157 (2012).

[26] A. M. Läuchli, E. J. Bergholtz, J. Suorsa, and M. Haque, Phys. Rev. Lett. **104**, 156404 (2010).

[27] Z. Liu, E. J. Bergholtz, H. Fan, and A. M. Läuchli, Phys. Rev. B **85**, 045119 (2012).

[28] S. Dong, E. Fradkin, R. G. Leigh, and S. Nowling, Journal of High Energy Physics **2008**, 016 (2008).

[29] L. Cincio and G. Vidal, Phys. Rev. Lett. **110**, 067208 (2013).

[30] E. H. Rezayi and F. D. M. Haldane, Phys. Rev. B **50**, 17199 (1994).

[31] E. J. Bergholtz and A. Karlhede, Phys. Rev. Lett. **94**, 026802 (2005).

[32] A. Seidel, H. Fu, D.-H. Lee, J. M. Leinaas, and J. Moore, Phys. Rev. Lett. **95**, 266405 (2005).

[33] I. P. McCulloch, "Infinite size density matrix renormalization group, revisited," (2008), unpublished, arXiv:0804.2509.

[34] M. B. Hastings, J. Stat. Mech. **2007**, P08024 (2007).

[35] D. Gottesman and M. B. Hastings, New J. Phys. **12**, 025002 (2010).

[36] N. Schuch, M. M. Wolf, F. Verstraete, and J. I. Cirac, Phys. Rev. Lett. **100**, 030504 (2008).

[37] M. Nakamura, Z.-Y. Wang, and E. J. Bergholtz, Phys. Rev. Lett. **109**, 016401 (2012).

[38] In the Supplemental materials we explain the numerical issues particular to quantum Hall iDMRG, including the MPO construction and ergodicity issues. We also detail the computation of the QP charges, flux matrices, and modular $\mathcal{T}$-matrix from the entanglement spectrum.

[39] U. Schollwöck, Annals of Physics **326**, 96 (2011).

[40] N. Read, Phys. Rev. B **79**, 045308 (2009).

[41] G. Moore and N. Read, Nuclear Physics B **360**, 362 (1991).

[42] We note that for bosonic states the $\mathbb{1}$ sector will not appear in the OES, a subtlety we address in the Supplement. For the fermionic states studied here, $\mathbb{1}$ will.

[43] E. H. Rezayi and F. D. M. Haldane, Phys. Rev. Lett. **84**, 4685 (2000).

[44] X.-G. Wen and Z. Wang, Phys. Rev. B **78**, 155109 (2008).

[45] E. Keski-Vakkuri and X.-G. Wen, International Journal of Modern Physics B **07**, 4227 (1993).

[46] J. E. Avron, R. Seiler, and P. G. Zograf, Phys. Rev. Lett. **75**, 697 (1995).

[47] X. G. Wen and A. Zee, Phys. Rev. Lett. **69**, 953 (1992).

[48] M. Levin, B. I. Halperin, and B. Rosenow, Phys. Rev. Lett. **99**, 236806 (2007).

[49] S.-S. Lee, S. Ryu, C. Nayak, and M. P. A. Fisher, Phys. Rev. Lett. **99**, 236807 (2007).

[50] L. Cincio and G. Vidal, In preparation.

[51] H.-H. Tu, Y. Zhang, and X.-L. Qi, "Momentum polarization: an entanglement measure of topological spin and chiral central charge," (2012), unpublished, arXiv:1212.6951 [cond-mat.str-el].